Charles University Prague
Faculty of Mathematics and Physics

BACHELOR THESIS

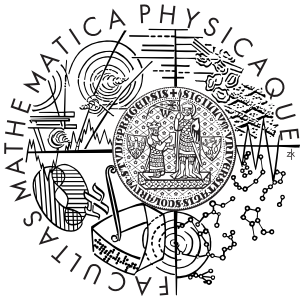

Tomáš Jindra

Development of semiconductor detectors for high energy physics experiments

Institude of Particle and Nuclear Physics

Supervisor: doc. RNDr. Zdeněk Doležal, Dr., ÚČJF MFF
Study Programme: General Physics

2010

I would like to thank to my supervisor Dr. Zdeněk Doležal for his leading of my bachelor thesis, for productive discussions and introduction into the problematics of semiconductor detectors. For help in building of the test setup I would like to thank all the members of the VdG accelerator lab at Institute of Particle and Nuclear Physics MFF UK, especially to ing. Peter Kubík for his help with technical aspects of ALIBAVA system. I'm very grateful to all fellow students who helped me with common problems during the whole year. Last but not least, I would like to thank to Daniel Červenkov, who processed ALIBAVA data and improved root macros for our laboratory.

I declare that I wrote my bachelor thesis independently and exclusively with the use of the cited sources. I agree with lending and publishing the thesis.

In Prague, 16^{th} July 2010 Tomáš Jindra

Contents

Název práce: Polovodičové detektory ve fyzice elementárních částic
Autor: Tomáš Jindra
Katedra (ústav): Ústav částicové a jaderné fyziky
Vedoucí bakalářské práce: doc. RNDr. Zdeněk Doležal, Dr., ÚČJF MFF
e-mail vedoucího: Zdenek.Dolezal@mff.cuni.cz

Abstrakt: Cílem předložené práce bylo podílet se na vývoji nových detekčních metod pomocí meření se zářičem. Za tímto účelem jsem se seznámil s principy detekce vysokoenergetických částic, s konstrukcí a funkcí křemíkových detektorů a osvojení metod vyčítání mnohokanálových detektorů. V práci jsem používal radioaktivní β^- zářič s jehož pomocí jsem postupně testoval v závislosti na různých parametrech odezvy scitilátoru, křemíkové diody a následně jsem se věnovat testování stripového křemíkového detektoru pomocí systému ALIBAVA. Nalezení vhodných parametrů pro měření, rozběhání systému a provedení prvotních testů bylo hlavním cílem celé práce a toto se nakonec zdárně podařilo.

Klíčová slova: Křemíkové detektory, Testy zářičem, Alibava

Title: Development of semiconductor detectors for high energy physics experiments
Author: Tomáš Jindra
Department: Institude of Particle and Nuclear Physics
Supervisor: doc. RNDr. Zdeněk Doležal, Dr., IPNP MFF
Supervisor's e-mail address: Zdenek.Dolezal@mff.cuni.cz

Abstract: Main goal of this bachelor thesis is to participate in development of new detection methods by measurements with radioactive source. For this purpose I have acquired knowledge of high energy particles detection, construction of silicon detectors and methods of readout multichannel detectors. Tests were made with radioactive ^{90}Sr source for different parameters and setup of scintillator, silicon diod and silicon microstrip detector with ALIBAVA system. The main aim of this work was to find out suitable parameters for measurement, set up ALIBAVA system and taking first tests.

Keywords: Silicon detectors, Source tests, Alibava

Chapter 1

Introduction

Semiconductor detectors have during these days a large field of applications. One of most important for high-energy physics is the purpose of precise position detectors of particle tracks in order of few μm. In presence of magnetic field the detectors allows very accurate momentum measurement. Relatively high energy loss of passing particles through the semiconductors provide possibility to create very small components with the size of μm. Semiconductors are also easily connected with readout electronics.

The detectors are usually required to work under high radiation, with spacial and cost limitation for the size and shape of detectors. At the same time they should be able to deliver the best results. This can be achieved through right development and choices to acquire sufficient parameters as position information, charge collection efficiency (CCE), time resolution, cluster size, pulse shape, signal-to-noise ratio (S/N) and others.

Detector testing includes using of a beam testing with high energy particles like in LHC, a laser testing and a radioactive source. The laser testing is not optiomal for optical character with some unwanted effects. The best conclusions may be obtained via the beam testing but due to the high cost and rare opportunities, β radioactive source is being used instead. Such testing is not limited by time or location as can be made with relatively undemanding equipment. On the other hand disadvantages of his method are continuous energy spectrum and bad spacial information.

For example the large hadron collider (LHC) is situated in the Center of European Nuclear Research (CERN). It contains 4 detector systems, one of them being the ATLAS with a semiconductor tracker (inner detector system) part consisting of silicon strips detector modules. The main function

of SCT modules is to precisely measure the momentum and the secondary vertexes position of charged particles with the short lifetime produced in a proton-proton collision. The properties of highly irradiated microstrip silicon detectors must be studied for achieving in the future a high luminosity at the SLHC (Super Large Hadron Collider) experiments. Particularly, the charge collected when a charged particle passes the detector is important for the detector performance. Its difficult to carry out complex testing and measurements. As a first step, a laboratory set up is needed but the measurements obtained with different setups could be not comparable if they are not calibrated correctly. Therefore an electronic system was developed which can acquire an analogue measurement (ALIBAVA). The Main goal for this system is reconstructing of the analogue pulse shape at the readout front-end chip with the maximum possible accuracy.

This bachelor thesis is focusing on principles and examinations of semiconductor detectors especially the construction and function of silicon detectors, what is the main content of *Chapter 3*. Just before this part is *Chapter 2* introducing basic of β decay as β radioactive source is implemented in all measurements.

The *Chapter 4* is dealing with scintillator detector and its properties as it will be used later for triggering both the silicon diode detector and as the trigger for the ALIBAVA system. *Chapter 5* is devoted to measurement with silicon diode detector and to observe the influence of trigger presence. Finally *Chapter 6* describes the setup and launching of ALIBAVA system for testing of microstrip detectors with presenting some of the first data and results.

Chapter 2

Beta decay

Usually good way to test or calibrate nuclear or high-energy physics detectors is by using a radioactive source. Suitable properties of emitted electrons are the reasons for using β source. Low cost and behavior of the most energetic electrons, which act like heavier particles with *minimum ionization* will be explained later in the chapter.

Beta radiation consists of fast electrons/positrons as a consequence of weak-interaction decay of neutron/proton in a nuclei under condition of excess of corresponding nucleon. According to production of electron or positron the β decay is marked either as β^- or as β^+ decay. For example in nuclei with majority of neutrons, neutron will undergo transformation into a proton. Correctly the process involves an electron and a electron antineutrino:

$$n \rightarrow p + e^- + \overline{\nu}_e \tag{2.1}$$

The proton remains incorporated in the nucleus while electron and antineutrino are emitted. Schematic representation of process is $(Z, A) \rightarrow (Z + 1, A)$. The second β^+ process is similar and proceeds in proton-rich nuclei with scheme $(Z, A) \rightarrow (Z - 1, A)$:

$$p \rightarrow n + e^+ + \nu_e \tag{2.2}$$

Consequence of the three particle decay is that the energy spectrum of β-particle is continuous. Reason for this is that β-particle and neutrino or antineutrino are sharing almost all available energy from decay. With assumption of small recoil energy of daughter nucleus and zero neutrino mass, the maximum energy of electrons should be approximate to the decay

energy. Majority of β sources have maximum value ranges from a few keV to a few MeV.

Some β sources have more than one decay branch or more precisely the daughter nuclei has different excited states. Also sometimes the daughter is still richer in favour of one nucleus type and may undergo another β decay or if the daughter nuclei is left in excited state it will deexcited by emission of one or more γ photons. Final spectrum is then superposition of particular branches and chains while respective contributions are weighted by their decay probabilities.

Because electron loss of energy in matter is relatively high, the β source should be thin. Under this condition emitted electrons lose minimum of energy during their escape from source matter.

For all measurements was used *Strontium* (^{90}Sr) source with activity 55,3kBq at the time of experiment. The decay chain for ^{90}Sr is showed below

$$^{90}Sr \xrightarrow{\beta^-} {}^{90}Y \xrightarrow{\beta^-} {}^{90}Zr \tag{2.3}$$

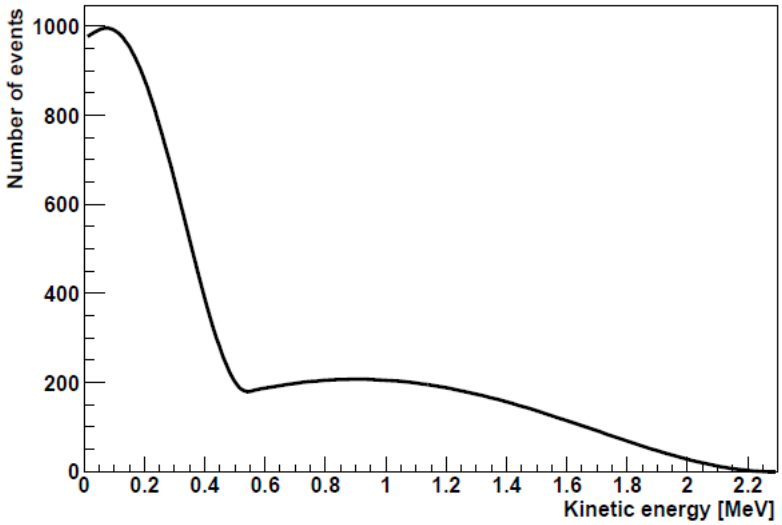

Figure 2.1: Energy spectrum of $^{90}Sr/^{90}Y$ source

and because of presence of two components source . Half-life time of ^{90}Sr is $T_{1/2_{Sr}} = 28.5$ year, while half-life time of ^{90}Y is $T_{1/2_Y} = 68$ hours. As $T_{1/2_{Sr}} \gg T_{1/2_Y}$ the number of decays are same for both ^{90}Sr and ^{90}Y.

According to [5] the maximum energy of e^- from ^{90}Sr is about 0.546 MeV and majority of these low energy electrons will stop in the detectors and deposit all energy there. The maximum energy of e^- from ^{90}Y is about 2.283 MeV and these electrons will usually pass through thin detectors while depositing only small fraction of energy according to Bethe-Bloch formula mentioned in section about interaction in semiconductors. Combined spectrum of both β-source is on figure 2.1 reproduced from [12].

Chapter 3

Semiconductor detectors

3.1 Comparison to other detectors

Common usage for semiconductor detectors in high-energy physics is for precise tracking. Especially important it is for detection of secondary vertexes of very fast decaying particle. For charged particle detection is the silicon the most used material and silicon detectors will also be used for measurements. Follow list of important features or advantages of silicon i.e. silicon detectors:

- A small value of the gap energy between valence and conduction band is 1.11 eV in silicon and so the average energy for creation of electron-hole pair (e-h) is 3.6 eV. This value is approximately 10 times lower compared to the ionization energy of gases used in proportional chambers, drift chambers and etc. And it leads to massive creation of charge carriers.

- High density of silicon is 2.33 g/cm^3 and due to this fact, the average energy loss per unit of length allows building thin detectors that still produce strong enough signal for measurement. For example in case of minimum ionizing particle (MIP) the energy loss is 390 eV/μm. High density also causes reduction of range of energetic secondary electrons which leads to better spacial resolution.

- The silicon detectors are mechanically rigid and therefore no special supporting structures are needed.

- The most of readout electronics is usually based on semiconductor technology. Due to this semiconductors can be connected with electronics which leads lower noise.
- High mobility of the charge carriers (electrons - 1450 $cm^2V^{-1}s^{-1}$, holes - 450 $cm^2V^{-1}s^{-1}$) means rapid charge carriers collection ($\ll$10 ns) and short dead time. Width of the readout pulse at half maximum (FWHM) is about 20 ns.
- Possibility of using semiconductor detectors in strong magnetic fields.

On other hand the semiconductor detectors pose some cons. High cost, radiation damage like in case of LHC or the fact that the output signal is only function of the detector thickness.

3.2 Silicon properties

Silicon belongs into IV group of the group of basic elements with Z = 14, A = 28.086 and crystallizes in a diamond lattice structure. Basis properties are described by a band model, electrons are detained in bands with different energy levels. For band structure see figure 3.1 [1].

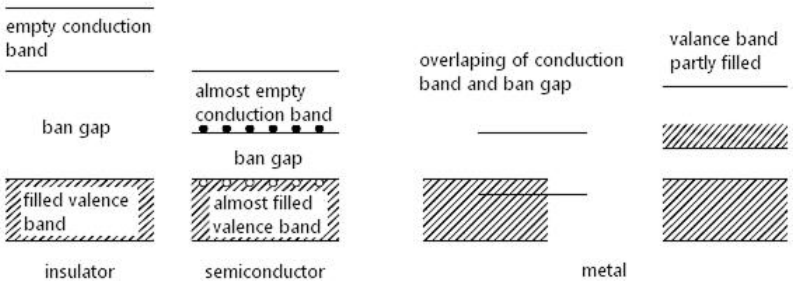

Figure 3.1: Band model for materials

The far-distant filled band is called a valence band, while the first empty band is called a conduction band. For silicon the valence band holds 4 electrons. Between these two bands lies band gap with no energy levels for electrons. The conductivity is then realized by electrons excitation from the

valence band into the conduction band. This may happen with higher temperature, when thermal vibrations breaks the covalent bonds of individual atoms and as result a leads to electron excitation. Electron excitation produce an empty state called hole, which behaves like a positively charged particle under electric field.

Both electrons and holes contribute to the total electric current. The semiconductor without impurities is called intrinsic and contains same densities of electrons and holes. Some atoms of silicon in lattice may be replaced with atoms from the III or V groups for getting materials known as a p- or n-type. Elements from the III group are known as acceptors and their valence band has 3 electrons and easily attach an electron from silicon atoms. Elements from the V group are known as donors and their valance band contains 5 electrons. One of these is very weakly bounded and can be easily excited to the conduction band. Semiconductors with a massive doping are marked as a $n+$ or $p+$ respectively. Due to the thermal excitation, both types of charge carriers appear in n- and p-type of semiconductors and they are called minority carriers. Band structure of both type is shown on figure 3.2 [1].

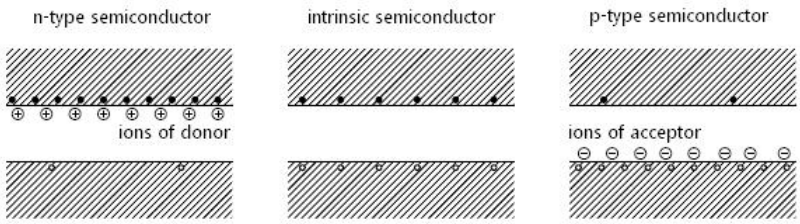

Figure 3.2: Comparison of semiconductors

The density of intrinsic charge carriers in thermal equilibrium is according to [11]:

$$n(T) = \int_{E_g}^{\infty} D_e(E,T) F_e(E,T) dE \tag{3.1}$$

where $D_e(E)$ is the state density [8]:

$$D_e(E) = \frac{1}{2\pi^2} \left(\frac{2m_e}{\hbar^2} \right)^{3/2} (E - E_g)^{1/2} \tag{3.2}$$

and $f_e(E)$ means the Fermi-Dirac function for system of fermions:

$$f_e(E) = \frac{1}{e^{\frac{E-E_F}{kT}} + 1} \approx e^{\frac{E-E_F}{kT}} \tag{3.3}$$

Where E states for the energy of electrons, E_F the Fermi level, E_g is the gap energy, T the temperature, k the Boltzmann constant, $\hbar$ the Planck constant and m_e is the effective electron mass.

Application of equations (3.2) and (3.3) in (3.1) and with use of relations for the density of holes $p(T)$,which is similar to the $n(T)$ provides relations:

$$n(T) = 2\left(\frac{m_e kT}{2\pi\hbar^2}\right)^{3/2} e^{\frac{E_F - E_g}{kT}} \tag{3.4}$$

similarly

$$p(T) = 2\left(\frac{m_h kT}{2\pi\hbar^2}\right)^{3/2} e^{\frac{-E_F}{kT}} \tag{3.5}$$

Silicon without impurities has the same number of holes and electrons per unit volume is the same ($n = p = n_i$) and do not depend on the Fermi level:

$$n(T)p(T) = {n_i}^2 = 4\left(\frac{kT}{2\pi\hbar^2}\right)^3 (m_e m_h)^{3/2} e^{\frac{-E_F}{kT}} \tag{3.6}$$

The relation (3.6) is still valid for doped silicon with densities N_A of acceptors or N_D of donors since only the Fermi level E_{F_e} changes in comparison with intrinsic semiconductor. The densities of extrinsic carrier follow equations coming from zero net charge density [13]:

$$n = n_i e^{\frac{E_{F_e} - E_F}{kT}} = 1/2\left[N_D - N_A + \sqrt{(N_D - N_A)^2 + 4n_i^2}\right] \approx N_D \tag{3.7}$$

and similarly

$$p = n_i e^{\frac{E_F - E_{F_e}}{kT}} = 1/2\left[N_A - N_D + \sqrt{(N_D - N_A)^2 + 4n_i^2}\right] \approx N_A \tag{3.8}$$

where particular approximations are valid for $N_D \gg N_A$ and n_i, $(n \gg p)$ in case of (3.7) and for $N_A \gg N_D$ and n_i, $(p \gg n)$ in case of (3.8).

Particle passing through the detector ionizes the Si atoms, producing effectively the e-h pairs. Typical thickness of silicon detector is about 300 μm so the number of generated e-h pairs by MIP passing perpendicular

Atomic number	14
Atomic weight	28.08
Atomic density	$4.99{\cdot}10^{22}$ cm^{-3}
Density	2.33 g/cm^3
Dielectric constant	11.6
Gap energy	1.11 eV
Effective states density in conduction band	$2.80{\cdot}10^{19}$ cm^3
Effective states density in valence band	$1.04{\cdot}10^{19}$ cm^3
Electron mobility	1350 cm^{2}V^{-1}s^{-1}
Hole mobility	480 cm^{2}V^{-1}s^{-1}
Electron Hall mobility	1670 cm^{2}V^{-1}s^{-1}
Hole Hall mobility	370 cm^{2}V^{-1}s^{-1}
Electron diffusion constant	34.6 cm^{2}s^{-1}
Hole diffusion constant	12.3 cm^{2}s^{-1}
Intrinsic carrier density	$1.45{\cdot}10^{10}$ cm^3
Breakdown field	30 V/μm
Diamond type lattice spacing	0.5431 nm
Mean energy for e-h pair creation	3.63 eV
Fano factor	0.115

Table 3.1: Properties of silicon at the room temperature ($T = 300K$)

through the detector is $3.2 \cdot 10^4$. This value is for comparison 4 order of magnitude lower than the total number of free carriers in intrinsic silicon of a surface of 1 cm^2 and the same thickness.

In doped material the signal to noise ratio (S/N) would be even smaller. Cooling of the semiconductor is one way to lower this ratio. An another one is by use of reverse biases P-N junction to deplete the detector of free carriers, which is the principle of the most silicon radiation detectors. Important properties of silicon are written in table 3.1.

3.3 Drift and diffusion

Several transport phenomena are at work in semiconductor materials. The most notable are the drift and the diffusion process and also the movement in magnetic field should be mentioned.

Drift of charge carriers means the movement of electrons and/or holes in

presence of external field $\vec{E}$. In case of weak external field, the drift velocity $\vec{v}$ is linearly proportional to the field:

$$\vec{v} = \mp\mu\vec{E} \tag{3.9}$$

where μ is coefficient of the proportionality. It represents mobility of electrons or respectively and is constant.

Movement of charge carriers in presence of magnetic field $\vec{B}$ results in the change of the movement direction by a Lorentz angle ϑ_L:

$$tan\vartheta_L = \mu_H B \tag{3.10}$$

where μ_H is coefficient is known as Hall mobility.

The diffusion is caused by not equal spacial variations of charge carriers distribution. Electron and holes move from point of high concentration to a point of low concentration and creating the diffusion flux $\vec{F}$:

$$\vec{F} = D\vec{\nabla}n \tag{3.11}$$

this equation shows proportionality of flow $\vec{F}$ to the density gradient $\vec{\nabla}$n using the diffusion coefficient D which is related to the mobility by Einstein equation:

$$D = \frac{kT}{q}\mu \tag{3.12}$$

where q is an elementary charge and T means the temperature.

3.4 The P-N junction properties

The basic concept used in semiconductor detector physics is the p-n junction. Its mainly allows current flow only in one direction. The p-n junction is created by composing together two extrinsic semiconductors of opposite doping. This results in creation of gradient of concentration that is causing carrier diffusion. Holes begin to diffuse from the p-side into the n-side and the electrons on the contrary. Since the number of acceptor ions N_A are fixed, uncompensated negative space charge in p-region near the junction will appear. Same is true for the uncompensated donor ions N_D will form positive space charge in n-region. This depletion region causes built-in potential barrier that, assuming $N_A, N_D \gg n_i$, can be obtained from [13]:

$$V_D = \varphi_n - \varphi_p = \frac{E_{F_A} - E_{F_D}}{q} = \frac{kT}{q}\ln\left(\frac{N_A N_D}{n_i^2}\right) \tag{3.13}$$

where φ_n is electrostatic potential of p-type region and φ_p is electrostatic potential of n-type region and E_{F_A} being the Fermi level in p-type semiconductor respectively E_{F_D} of n-type. For the illustration of P-N junction see figure 3.3 [6].

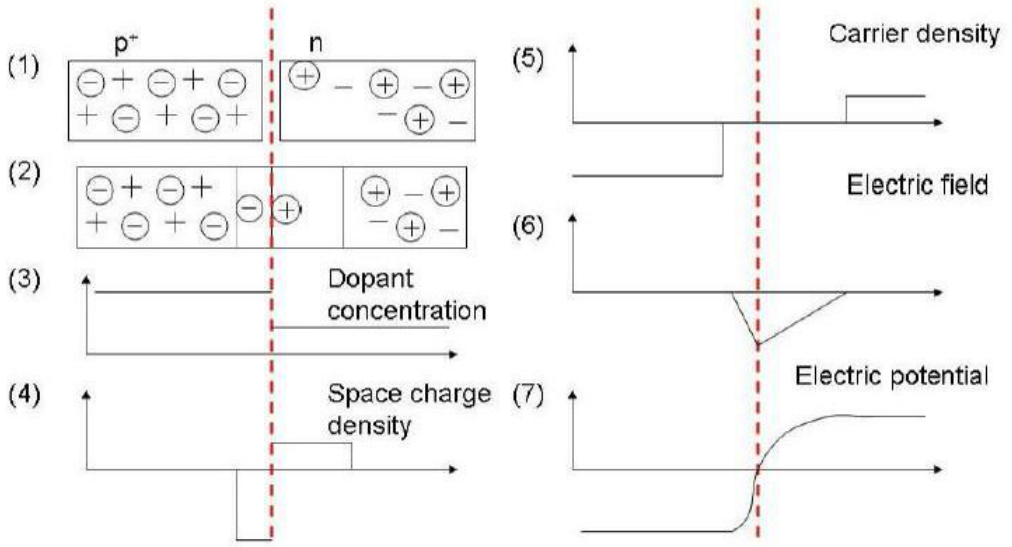

Figure 3.3: P-N junction 1) p and n-type material 2) P-N junction in thermal equilibrium 3) absolute doping concentration 4) space charge density 5) free carrier density 6) electric field 7) electric potential.

For practical use the depletion region can be extended by applying reversed potential V_{bias} on the P-N junction, which will reflect in increase of barrier height to $V_B = V_{bias} + V_D$. The electric field distribution can be obtained by solving a one-dimensional Poisson equation:

$$\frac{d^2V(x)}{dx^2} = \mp\frac{qN(x)}{\epsilon} \tag{3.14}$$

where ϵ is electrical permittivity of Si.

Mark χ_p and χ_n as the width of depletion areas for p-type region and n-type respectively. With consideration of space charge neutrality of the P-N junction in case of equal space charge densities [13]:

$$N_A\chi_p = N_D\chi_n \tag{3.15}$$

the partial depletion depth can be obtained:

$$\chi_n = \sqrt{\frac{2\epsilon}{q}\frac{N_A}{N_D\left(N_A+N_D\right)}V} \tag{3.16}$$

$$\chi_p = \sqrt{\frac{2\epsilon}{q}\frac{N_D}{N_A\left(N_A+N_D\right)}V} \tag{3.17}$$

and the total depletion depth:

$$W = \chi_p + \chi_n = \sqrt{\frac{2\epsilon}{q}\frac{\left(N_A+N_D\right)}{N_A N_D}V} \tag{3.18}$$

Another characteristic for P-N junction is a depletion capacitance C. The capacitance is related to an increment of charge dQ created on both sides of the junction after the change of external voltage:

$$dQ = qNdW \tag{3.19}$$

$$C = \frac{dQ}{dV_B} = \frac{dQ}{dW}\frac{dW}{dV_B} = \sqrt{\frac{q\epsilon N_A N_D}{2(N_A+N_D)V}} \tag{3.20}$$

The capacitance C is decreasing with higher bias voltage until depletion layer spreads to the back of the crystal.

With increasing bias voltage the depletion area will spread until it reaches the back of the semiconductor crystal. Such a V_B is called depletion voltage V_{dep}. The depletion region is almost without majority carriers, but under equilibrium conditions $e-h$ pairs are still generated within the semiconductor. The created carriers have little chance to recombine. The pairs are separated and electrons and holes drift under the influence of the electric field and it is known as *leakage* or *reverse current*. Depending on point of the $e-h$ creation, two components may arise: a generation current of density j_{gen} caused by charge carriers created within the depletion zone and a diffusion current j_{dif} coming from charge created in the neutral region and diffusing into the depletion zone. First one depends strongly on the temperature and the second one on the recombination time for particular carriers and it is proportional to the contact area of the junction.

3.5 Reversed bias junction

P-N junction described above does not provide the best operating characteristics. The intrinsic electric field will not be strong enough to provide efficient charge collection and the thickness of the depletion zone will not be adequate for high-energy particles. Improvement can be reached by use of a reverse-bias voltage to the P-N junction. This time negative voltage is applied to the p-side and positive to the second one. Holes in the p-region are attracted from the junction towards the p contact and similar is true for electrons and the n contact. This effectively spread the depletion area and therefore the sensitivity for particle detection. Higher external voltage provides a better charge collection.

3.6 Interaction of particles in silicon

Free charge carriers are created in the semiconductor by excitation of electron from valence band to the conduction band. This either left a hole in the valence band which behaves as positive charge. Energy for the excitation can be obtained by different ways. For example thermal movement (thermal excitation), absorption of photon quantum (optical excitation) or by interaction with passing ionizing particle.

Thermal excitation does not require any other form of starting impulse. This phenomenon occurs just by room temperature (kT≈0.026eV). It is causes by impurities, irregularity in structure lattice or by dopant. Thermal excitation results in the detector noise and. Active cooling is a method to deal with it especially for semiconductors with small ban gap (Germanium). Detectors based on the silicon have sufficiently low noise even by room temperature

Optical excitation is consequence of single photon absorption and means creation of one $e - h$ pair due to the fact,that the energy of light of visible light spectrum is comparable with width of ban gap.(400-700nm wave length $\approx$ 3-1 eV)

For charged particles there are two mechanisms of energy loss in solid matter: heavy particles lose energy mainly by the ionization, while for light particles e.g. electrons is in play also bremsstrahlung. Part of the ionization process is the releasing of high energy electrons (δ-electrons) that increase the mean energy loss. Another important effect is the Coulomb scattering resulting in altering particle direction after passing through the detector.

The mean energy loss due to ionization is described by Bethe-Bloch formula [9]:

$$-\left(\frac{dE}{dx}\right)_{ion,e^-} = 2 \cdot \frac{2\pi\alpha^2\hbar^2 z^2}{m_e\beta^2}\frac{Z}{A}N_A\rho\cdot\ln\left(\frac{T_{max}}{T_{min}}\right) \tag{3.21}$$

where z is charge of particle, M is mass and velocity is $\beta = \sqrt{1-\gamma^{-2}}$ in units of speed of light c. T states for energy loss, m_e for electron mass, Z/A for atomic number/weight of material with ρ density. α is the fine structure constant and N_A is the Avogadro constant. The minimum energy loss T_{min} is equal to the ionization potential $I_0 \approx 16 \cdot Z^{0.9}$ and maximum energy T_{max} loss is defined as:

$$T_{max} = \frac{2m_e c^2\beta^2\gamma^2}{1 + 2\gamma\frac{m_e}{M} + \left(\frac{m_e}{M}\right)^2} \tag{3.22}$$

And modification of the Bethe-Bloch formula for fast electrons:

$$-\left(\frac{dE}{dx}\right)_{ion,e^-} = \frac{2\pi\alpha^2\hbar^2 z^2}{m_e\beta^2}\frac{Z}{A}\rho N_A\,[...] \tag{3.23}$$

where [...] is:

$$\left[\ln\left(\frac{m_e^2 c^4\beta^2\gamma}{2I^2(1-\beta^2)}\right) - \ln 2\left(\frac{2}{\gamma} - \frac{1}{\gamma^2}\right) + \frac{1}{\gamma^2} + \frac{1}{8}\left(1 - \frac{1}{\gamma}\right)^2\right] \tag{3.24}$$

Due to the stochastic nature of the energy losses, large statistical fluctuations can appear in the amount of energy deposited by the incident particle especially in thin detectors. The character of ionization fluctuations are described by Landau, Vavilov or Gaussian theory in a detector of thickness δx depends on ration ξ,which is proportional to the ratio of mean energy loss to the T_max:

$$\kappa = \frac{\xi}{T_{max}} = \frac{2\pi\alpha^2\hbar^2 N_A z^2 Z\rho}{m_e\beta^2 A} \cdot \frac{\delta x}{T_{max}} \tag{3.25}$$

For Landau theory is valid assumption that the ratio $\xi/I_0 \gg 1$ and for small energy loss in comparison with T_{max} but is large enough in comparison with the binding energy of the most bound electrons. The first restriction is removed in the Vavilov theory. Landau theory thereby can be used when κ <0.01 and Validov theory for 0.01< κ <10. κ >10 describes nonrelativistic particle energy loss and for this parameterization can be used Gaussian distribution, assuming a large number of collisions, which results

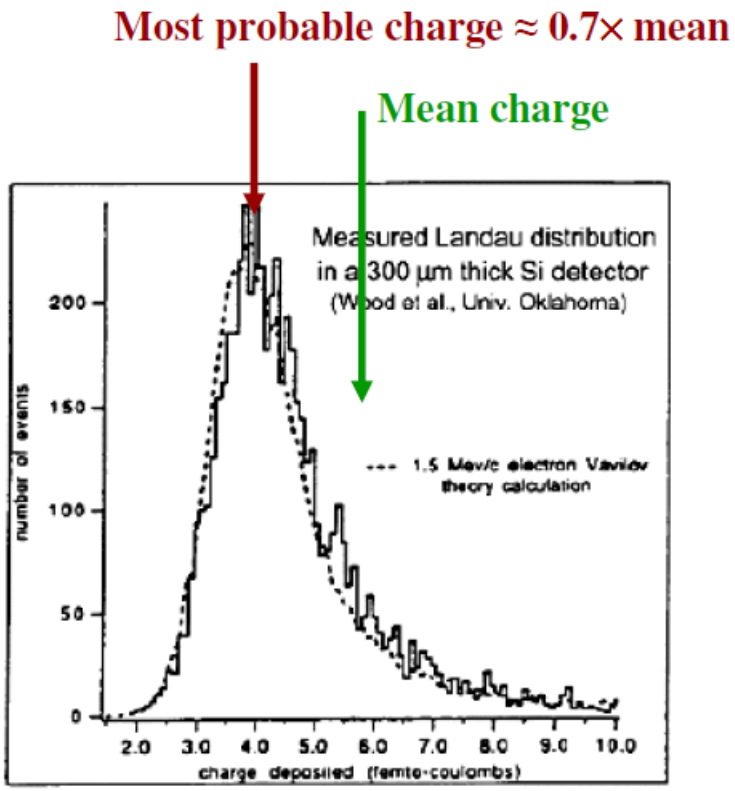

Figure 3.4: The Landau distribution

in the loss of most of the incident particle energy. For Landau distribution see figure 3.4 [6].

The high energy tail at the energy loss in Landau distribution is caused by high energetic δ-electrons, which are resulting in major increase of average energy loss than is the most probable value. On the other hand the range of δ-electrons is in order of 10μm, which can affect the measured track position of incident particle. The second mechanism of energy loss important for $e^{\mp}$ is releasing of electromagnetic radiation called bremsstrahlung and is described by the formula [9]:

$$-\left(\frac{dE}{dx}\right)_{brem,e^-} = \frac{\alpha^2\hbar^2\gamma Z\left(Z+1\right)N_A\rho}{137m_eA}\left[4\ln\left(2\gamma\right)-\frac{4}{3}\right] \tag{3.26}$$

The relative influence of ionization and bremsstrahlung in solid materials is

described by critical energy according to[5]:

$$E_c = \frac{610}{Z + 124} \cdot MeV \tag{3.27}$$

3.7 Silicon diode detectors

As was mentioned in previous sections, silicon has advantages of room temperature operation and wide cheap availability. On the other hand, disadvantage is their relatively small size. The most used silicon detectors for charged particle measurements are of *surface barrier type*. In this case the junction is formed between a semiconductor and a metal, usually n-type silicon with gold (such as a detector we will use for tests) or p-type silicon and aluminium.

Situation is similar to P-N junction but now the depletion zone is extending only into the semiconductor part. The thickness of depletion zone may varied. In case of not too thin detector, full depletion is possible for silicon and allows measuring of the deposition energy of passing particles. Higher bias voltage on fully depleted detector further provide faster signal due to a gain in the collection time of charged carriers.

Disadvantages of surface barriers detector is that they provide no position information about incident particles. Another one is their sensitivity to light as thin metal layer is not enough to stop light. Therefore these detectors should be use in some sort of shielding or box. The last disadvantage is sensitivity to surface contamination, so they should be handled with care as all others [10].

3.8 Microstrip detectors

Semiconductor devices are in present-days used as high-resolution spacial detectors (the tracking detectors) in comparison Particles traveling through the detector create a number of e-h pairs along its path and it is adequate to the energy loss described in *section 3.7*. The silicon microstrip detectors are using the phenomenon of reverse biased P-N junction with full depletion. It consists of weakly doped n-type bulk with $p+$ strips implanted in it and with aluminium strips that serve as good ohmic contacts between n-type substrate and $p+$ layer. Scheme of typical n-type microstrip detector is shown on figure 3.5.

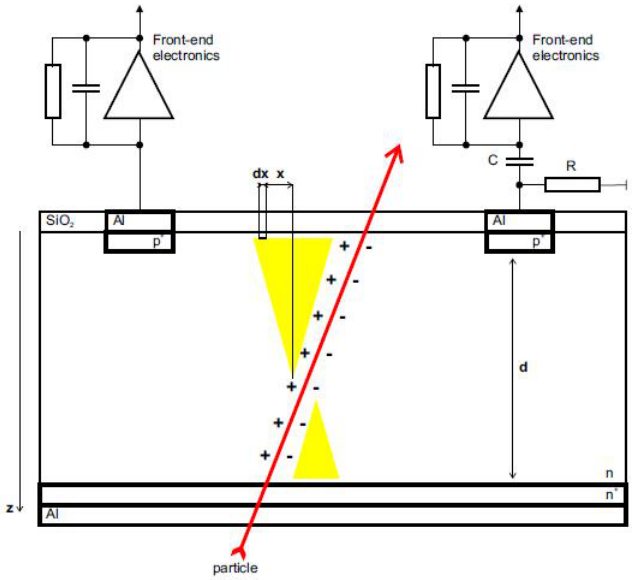

Figure 3.5: n-type microstrip detector with DC-readout on the left side and AC-readout on the right as is shown in [12]

Analog readout allows measuring the amplitude of the signal on each particular strip. This allows partial reconstruction of the spacial distribution and that provides better localization precision compared to the strip pitch p of the microstrip detector:

$$\Delta x \approx \frac{p}{S/N} \tag{3.28}$$

The induced signal on a strip is compared with the threshold level. Using a binary readout and analysis, the root mean square (RMS) of the measured track position is obtained. The measurement precision Δx^2 can be calculated under condition of no charge loss as:

$$\left\langle \Delta x^2 \right\rangle = \frac{1}{p}\int_{-p/2}^{+p/2} x^2 dx = \frac{p^2}{12} \tag{3.29}$$

Advantage of semiconductor detectors as mentioned in *section 3.1* is about an easy connection between semiconductors and electronics. There are two possible ways how the division of charge between strip can be realized. The resistive method means a noise generation but reverse current flows

through the electronics. The capacitive method means charge loss because of strip-ground and strip-to-strip capacitance and where only current changes are detected by the electronics. This method is realized by the interstrip capacitance and result in non-linear response of detector. Noise characteristic is one of important properties of microstrip detectors for performance. Noise is mainly caused by the front end electronics and by the detector capacitances.

3.9 Radiation damage

Semiconductor detectors are sensitive to radiation. Incident particles collide with lattice atoms and cause that way point defect by alteration of atom position. This leads to permanent material changes that act as discrete trapping centers reducing signal and as recombination centers. There also appear to be changes in resistivity, which result in the requirement of higher depletion voltage.

The main consequences of the radiation damage are an increased leakage current and degradation of energy resolution. leading to an increase of the leakage current. Majority of the primary defects are mobile at room temperature and will anneal in time.

Chapter 4

Measurement with scintillator

4.1 Motivation

Motivation for this experiment with a scintillator detector is to determine parameters for further measurements where scintillator will serve as part of trigger. The important property is how depends number of detected events on the different distance between β radioactive source and the scintillator. Similar is true for control voltage applied to the photosensor.

4.2 Scintillation detectors

These days scintillation detectors are one of the most common and most widely used device for detection of particles in nuclear and particle physics. Basic concept of scintillators is that some materials under hit of a radiation or nuclear particle produce a small flash of light which is called a scintillation. In order to convert scintillation and amplifying is usually scintillation detector coupled with photomultiplier. This way is a light flash transformed into electrical pulses for further analysis often to obtain information about incident radiation.

4.2.1 Characteristics of scintillators

Scintillator detectors consist of scintillating material part and photomultiplier. These two parts are usually optically coupled directly or with help of a light guide. Passage of radiation through the scintillator causes light emission. This happens due to excitation of atoms or molecules from which

the scintillator consist of. Flash of light is transmitted to the photomultiplier (PM/PMT for short) where it is converted into a weak current of photoelectrons which is further amplified.

Linear response of scintillators according to deposited energy of incident particle is a good approximation. In fact, the response depends not only on energy. For example the type of particle and its particular ionization may influence this response.

Also temperature may influence light output of scintillators. Dependence is generally not important at room temperature where measurements will take place.

The signal from scintillator is able to provide some interesting information. For example:

- *Fast Response Time*. In comparison with response of other detectors the scintillators are fast devices due to their quick response and short recovery times. This feature allows timing information for example serving as part of trigger or for higher count rates due to short dead time of scintillators.

- *Energy Sensitivity*. When incident particle or radiation deposited energy above fixed minimum in scintillator, the response of most scintillators will be adequate to this energy. Proper usage of multiplier with linear effect will provide proportional amplitude of output electrical signal in comparison with deposited energy. Therefore scintillators could be used as energy spectrometer.

- *Pulse Shape Discrimination*. Some kinds of scintillators allows to distinguish different types of incident particles by producing different shape of emitted light pulses which follow to different electric shape pulse. Reason of this phenomenon is different excitation mechanisms cause by various particles and various energy.

Scintillators hold property of *Luminescence*. Luminescent materials after exposition to radiation,light,heat or another form of energy absorb and then reemit the energy in the form of visible light. *Fluorescence* means reemission immediately after absorption within 10^{-8}s. Delayed emission can occur if excited state is metastable and in this example its called *phosphorescence*. However the delay time may be between microseconds and hours depending on the material. There is number of materials used for scintillators with various advantages or disadvantages like plastics, inorganics crystals, organic,

organic crystals, organic liquids, gases or glasses. While suitable material for detector should fulfill criterion as:

1. High efficiency for conversion of exciting energy to fluorescent radiation.

2. Transparency to its self fluorescent radiation, allowing light transmission into photomultiplier.

3. A short decay constant.

4. Emission in spectral range sensible for photomultipliers.

For measurement a plastic scintillator (organic principle) will be used as they the are providing a very fast signal and high light output. Another advantage of plastics is their flexibility to be produced in desired forms and shapes.

4.2.2 Intrinsic detection efficiency

Not all combinations of scintillator detectors and various radiation produce usable signal. Mechanism of interaction varies and so must be considered in order to get usable probability of interaction, response of light output. Another important parameter is mean free path of the radiation in the scintillator material. Charged particles with not too high energy have this distance on the microscopic level and so its probability to lose energy in the most of scintillators with normal dimension is close to 100%. For neutral particles is mean free path usually greater but that is not problem while using β radioactive source. Only few of electrons will fail to produce a detectable signal. On contrary, due to small mass of electrons the effect of backscattering/sidescattering or large angle scattering in matter may appear. These effects prevent full energy deposition.

The effect of backscattering depends strongly on the atomic number of the scintillator material. Dependence is rapidly increasing with higher Z.

Electrons with very high energy loss energy mainly through the production of bremsstrahlung and the consequent electron showers. For successful production of showers is needed a material with high-Z. Due to atomic number and density the inorganics scintillators are preferred.

4.3 Photomultiplier

Photomultipliers (PM´s) are electron tube devices which ensure conversion of light into a measurable electric current. They are usually and widely used in nuclear and high-energy physics because of high sensitivity. The most often photomultipliers are mentioned with scintillator detectors, even though their usage can varied.

Photomultipliers are assumed to have linear response. The output current of PM is directly proportional to the number of incident photons. A scintillator produces photons in proportion to the energy deposited in the scintillator. Device created by coupling a scintillator to a PM would be capable of providing information on the particle detection and also the energy it has loss in the scintillator detector.

Because of high photosensitivity of PM, it is dangerous to expose the PM to ambient light while it is under voltage. It is best to avoid exposure the PM to excessive illumination even when not under high voltage.

4.4 Scintillation detector mounting and operation

The hard part of working with scintillation detectors is mounting of scintillator and photomultiplier. Wrong fashion causes problem with collection and transport of light between components. Light from a scintillator can be lost due to two processes. First is escape through the scintillator boundaries and the second one is by absorption by scintillator material. The second one means problem only for large dimensional scintillators. Light is emitted at any point in the scintillator and then travels in all directories so only small fraction of emitted light passes into PM. Different point of light origin causes that response is not equal for the same particle however this dispersion is negligible for devices used in nuclear physics.The voltage applied to the PM determines more or less the gain and therefore pulse height of the output signal.

Coupling of scintillator and PM needs to allow a maximum of light transmission into PM. For this reason is not desirable to leave air or dirt between these two parts. As it will result in lowering of the light transmission. Suitable optical contact is therefore made of material with similar index of refraction as a scintillator and the PM (silicon grease or oil).

4.5 Experiment setup

As radioactive source serves the same one Strontium ^{90}Sr source as for testing of silicon detector and ALIBAVA system with activity 55,3 kBq at the time of measurement. This isotope is one of the best long-lived high-energy beta emitters know in nature.

Because the source has areal circle shape with 5mm diameter we will use collimator for experiment to get as much as possible collimated beam of electrons from the source. The collimator has height 24mm and diameter 2.5mm. Thanks to mechanical setup the distance between scintillator and the source is changeable. The minimum position means distance 35mm while maximum is 75mm. Because setup provides only mechanical arrestment without any locking position for collimator the distance is determined with error of 1mm at the best. Yet all measurements with the same distance between RS and scintillator were taken without changing or modifying of collimator position. For layout see figure 4.1.

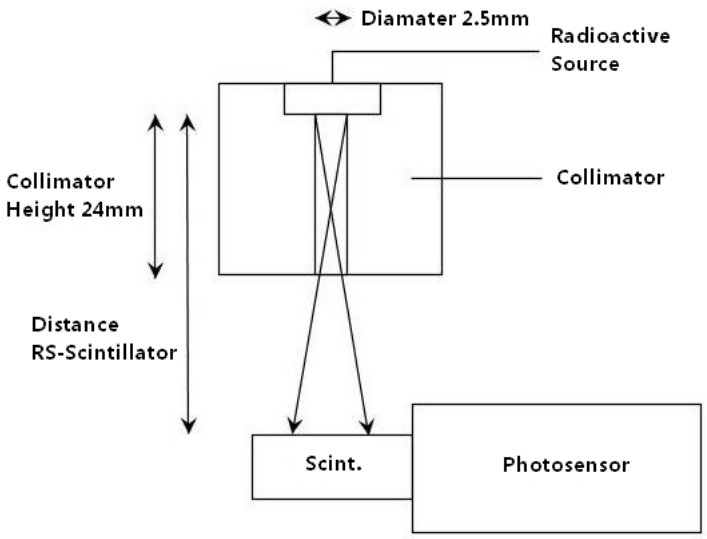

Figure 4.1: Scheme for geometry and position of RS and Scintillator

For this measurement is used typical HAMAMATSU photosensor module H5783-01 with plastic scintillator. The experiment takes place in metal black box to prevent interference with lighting in laboratory room. The

H5783 are photosensor modules housing a metal package PMT and high-voltage power supply circuit. The metal package PMTs have a metallic package with the same diameter as used for semiconductor photodetectors, and deliver high gain, wide dynamic range and high speed response while maintaining small dimensions identical to those of photodiodes. The internal high-voltage power supply circuit is also compact, making the module easy to use. Dimensional outlines are on figure 4.2. Dependence of photosensor gain is linear function of applied control voltage as is showed on figure 4.3.

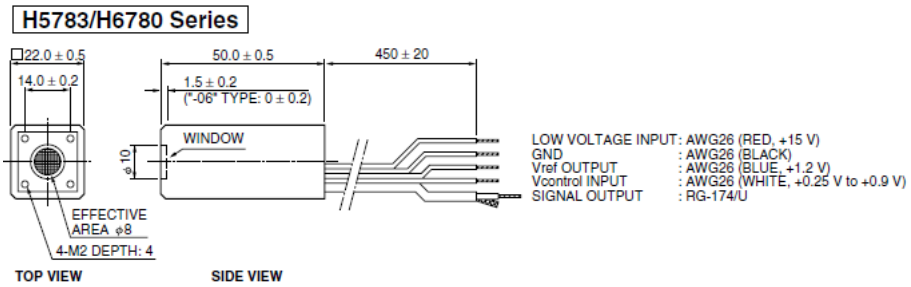

Figure 4.2: Dimensional outlines of the photomultiplier H5783

Photosensor module has five connections. *Reference voltage output* is used to control the gain with a variable resistor and is set to 1.2V. *Reference voltage input* supply a voltage (DC voltage) for controlling the gain of the photosensor module. Increasing the control voltage increase the voltage applied to the build-in photomultiplier tube and so increase the gain. For this model recommended control voltage range is from 0.25V to 0.90V. *Power supply input* (low voltage input) is DC voltage required for function of photosensor module. For this task dedicated power supply of +15V is used. *Power supply ground* is internally connected to the case and should be connected to the external power supply ground. The last is *Signal output* which provides output from the photosensor module. It is internally connected to the output of the build-in photomultiplier tube. Informations taken from [4].

The output signal from the scintillator is multiplied by photosensor module and consequently processes by *discriminator*. The discriminator responds only to an input signals with a pulse height greater than a certain threshold value. If the signal is high enough, the discriminator will produce a standard logic signal. If not, no response is then made. The level of threshold can be usually preset directly on the module. As well, an adjustment of the

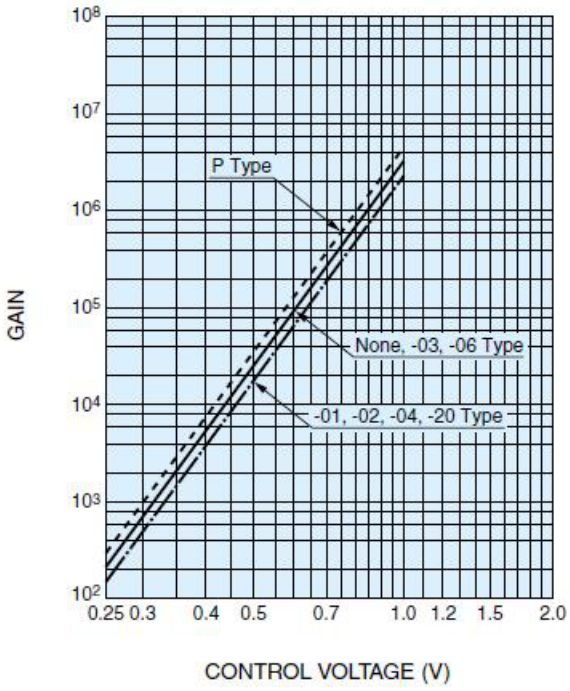

Figure 4.3: Gain of photosensor as a function of control voltage

width of the logic signal is usually possible via similar controls. The most common usage of discriminator is for blocking low amplitude noise pulses from photomultipliers etc. Pulses with height above threshold level trigger discriminator and are transformed into logic pulses for further processing by next electronics as states [10].

The last part of setup is *time counter* which sums up the number of logic signals from discriminator alias number of detected events by scintillator. As counter serves *Dual Counter/Timer Model 512* made by Canberra Nuclear. This module also provides possibility to set time for which signals should be gathered for comparison of different settings and parameters of whole experiment with scintillator detector. Scheme of the whole experiment with scintillator detector is on figure 4.4.

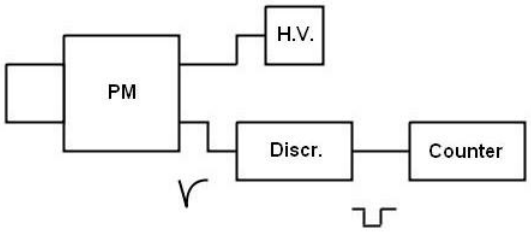

Figure 4.4: Scheme of connected modules with shape of output signals

4.6 Results

To use scintillator as trigger for following test the knowledge of background level is important. For good triggering majority of detected events should be caused by electrons from the radioactive source and only minority by background radiation as cosmic radiation or lighting in laboratory room.

First measurement handles this problem. After several trials the time period for particular measurements was determined as 500s. Background test proceeded with fixed 35mm spacial distance between RS and scintillator and with fixed value 0.9V control voltage of photosensor. As is seen on figure 4.5 the background is lowering with higher threshold of photosensor module. In comparison with RS signal with same parameters (fixed spacial distance, fixed control voltage and for the same values of threshold level) the background is negligible and thus signal from scintillator could be used as trigger in future with good credibility. For comparison of signals see figure 4.6 in logarithmic scale.

After determination of background tests were made cross-likely to cover various parameters - how much detection is made with scintillator in different spacial position starting in distance 35mm and ending with maximum possible distance of 75mm. How depends number of events on threshold level and control voltage of photosensor module. Results for these tests are summed up and shown on figures 4.7,4.8,4.9. As expected events detection is intensely lowering with higher threshold and lower control voltage. While dependence on spacial distance seems to be almost linearly decreasing for fixed control voltage and threshold level.

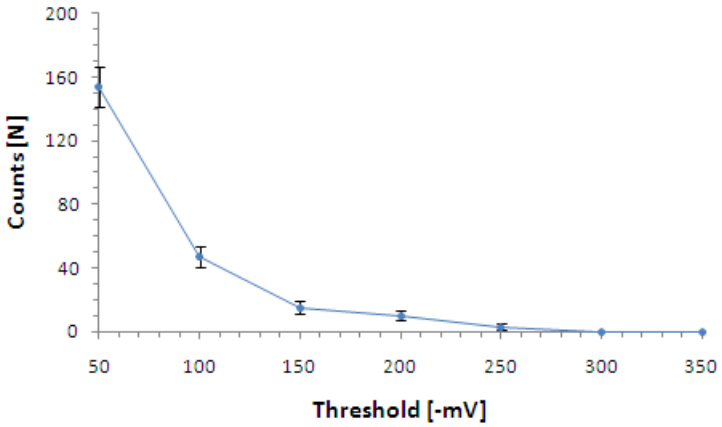

Figure 4.5: Background signal of scintillator with different threshold level and no RS

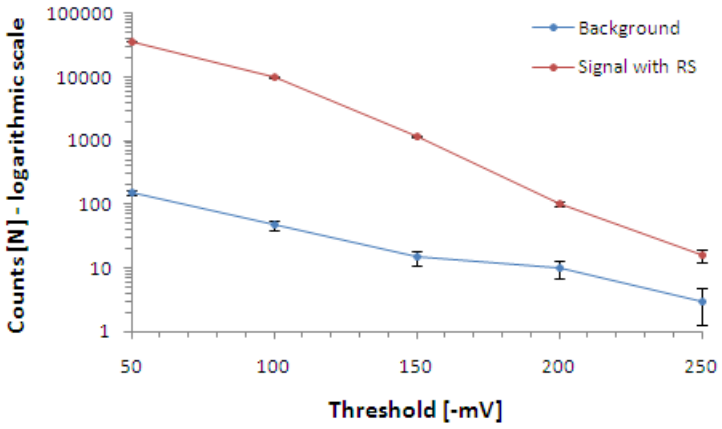

Figure 4.6: Comparison of background and radioactive signal for different threshold and control voltage 0,9V

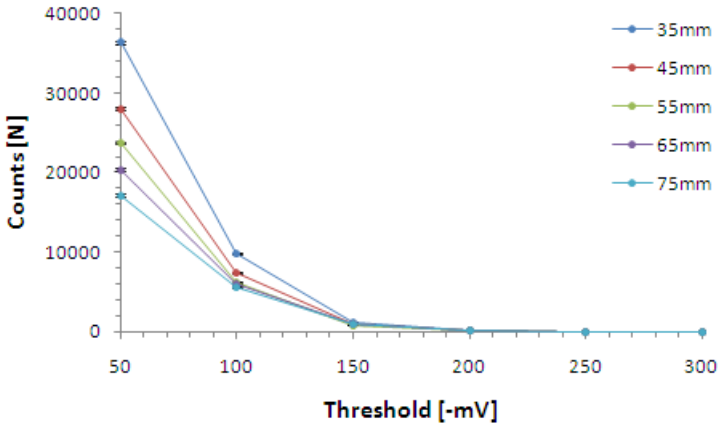

Figure 4.7: RS signal for different threshold levels and distance and fixed control voltage $0,9V$

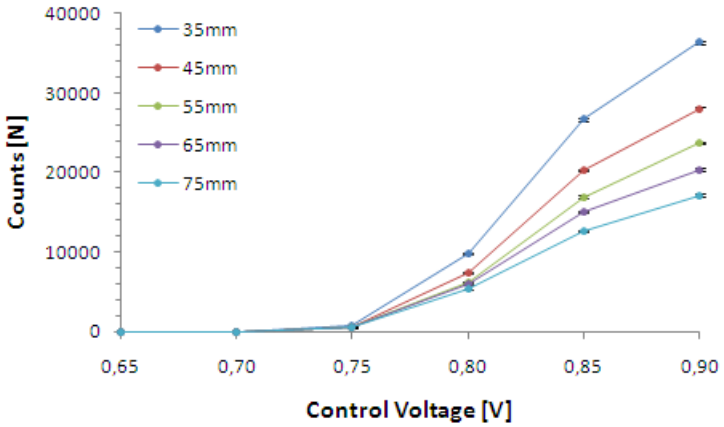

Figure 4.8: RS signal for different control voltage and distance and fixed threshold level -50mV

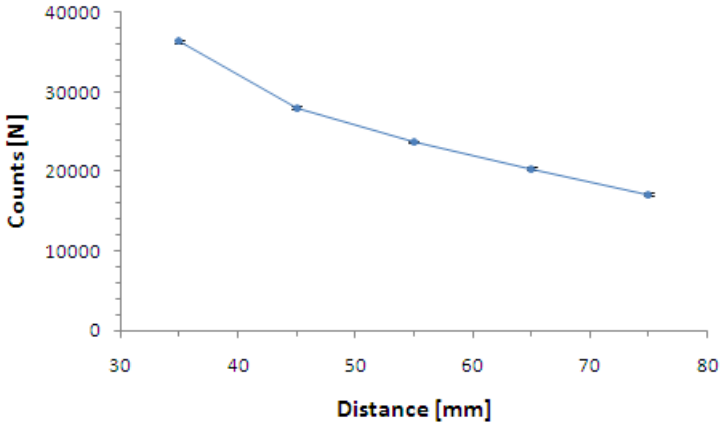

Figure 4.9: RS signal for different distance and fixed setting of threshold -50mV and control voltage 0.9V

Chapter 5

Measurement with silicon diode

The detail properties of the semiconductor detectors and the silicon diode were discussed in *chapter 3*. The radioactive source will be $^{9}0$Sr with maximum energy 2.3MeV for electrons. The most energetic electrons pass through diode and are registered by the scintillator. The fast signal from scintillator is then used as trigger for slower signal from diode. For this kind of detectors is no way of deducing a particles interaction point except to say that is happened within the detector. The output signal will depend on the type of ionizing particle interacting in the detector and the depletion width , which is corresponding with the applied bias voltage.

Electrons have continuous energy spectrum as described in *chapter 2* but cannot be considered to act as minimum ionizing particles (MIP). The low-energy electrons are completely stopped in diode and deposit there the whole energy (according to Bragg curve hundreds of keV), while the most energetic ones will pass only with small loss of energy (under 100keV). These electrons can be compared to the MIP as they deposit about 70keV in typical 300μm thick layer of silicon. This is reason for implementing the trigger system. Using a threshold will allow only the most energetic electrons to activate the trigger. Increasing of threshold will effectively result in blocking the low energetic electrons.

5.1 Experiment Layout

The first part of "the trigger branch" is without changes. The properties and description of scintillator, photomultiplier, discriminator were made in *chapter 3*. Only their function will be mentioned here - to obtain a fast signal of the passing particles for triggering the detector signal. The counter is used for retrieving information about number of events in selected time window.

New modules add to the trigger branch are *dual timer* for delaying and widening of signal, *level adapter* for changing polarity of signal, *linear gate stretcher* to prolong the duration of analog signal at the peak value. The Reason is to shape the fast signal in order to be accepted by MCA. The complete scheme for experiment is on figure 5.1

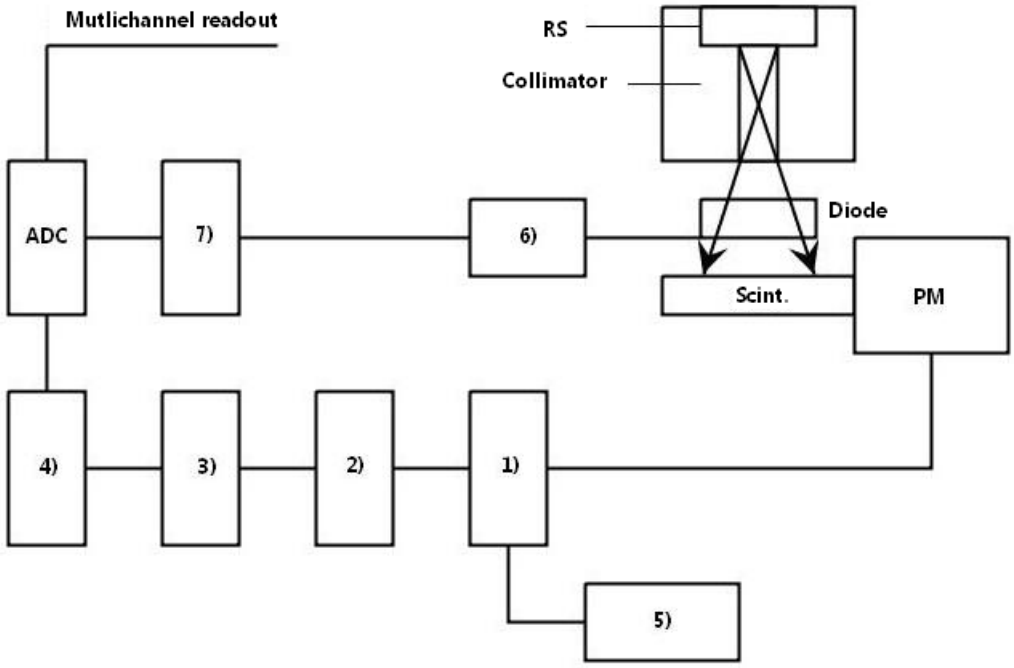

Figure 5.1: Scheme for measurement with diode - modules: 1) discriminator 2) dual timer 3) level adapter 4) linear gate stretcher 5) counter 6) preamplifier 7) amplifier

5.1.1 Preamplifier

Signal from semiconductor detector has small amplitude, so preamplification is required for further processing of the signal. The important property of the preamplifier is the noise, as it influence the resolution of the detector. The noise is described by *equivalent noise charge* (ENC) as signal from detector is obtained in form of electric charge.

$$ENC = e\frac{V_{rms}}{w}C \tag{5.1}$$

where w is average energy for creation of $e-h$ pair, C is total capacitance of the detector and preamplifier and V_{rms} is the average voltage noise level at output. Therefore the preamplifier is mounted as close to the detector as possible to lower the capacitance of cables. In case of particle spectroscopy under room temperature is usually used ADC method of signal processing. In this configuration is one electrode of the diode grounded by mounting but another load capacitor is affected the noise as is discussed in [10].

5.1.2 Main Amplifier

Main amplifier allow further amplification of the signal (gain) and shaping to a more suitable form for processing. Energy spectroscopy required that the output signal amplitude must be strictly proportional to the input signal amplitude.

One important factor is pule shaping time. The incoming pulse signal from preamplifier is in shape of exponential with long tail with time period τ, while the pulse height corespondent with energy. Problem arises when another signal appears during τ of the first signal. In that case the energy information about second signal is compromised. This is known as *pile-up* effect. Solution is to shorten the signal by shaping time.

5.1.3 MCA and ADC

Main objection for multichannel analyzer (MCA) is sorting of incoming signals according to their value, storing them in memory and counting content for each channel. MCA is working with a digital information and therefore ADC was implemented to process the analog signal for MCA. Using calibration of well-known spectrum like ^{241}Am (α radioactive source) allows measuring of unknown spectrum. (*System* 100 *from Canberra Nuclear*) will be use for our measurements.

5.2 Signal shapes and timing

All previously mentioned modules are used for alternation of signals from scintillator and diode detector. The main goal is to use the fast signal from

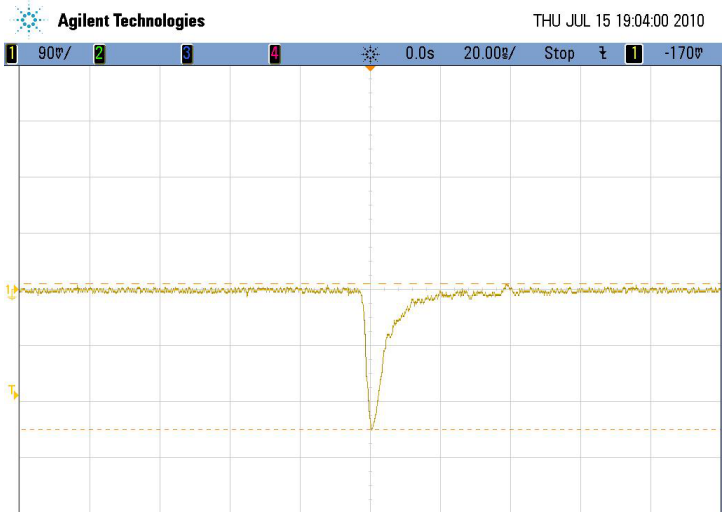

Figure 5.2: Signal from photomultiplier (scintillator)

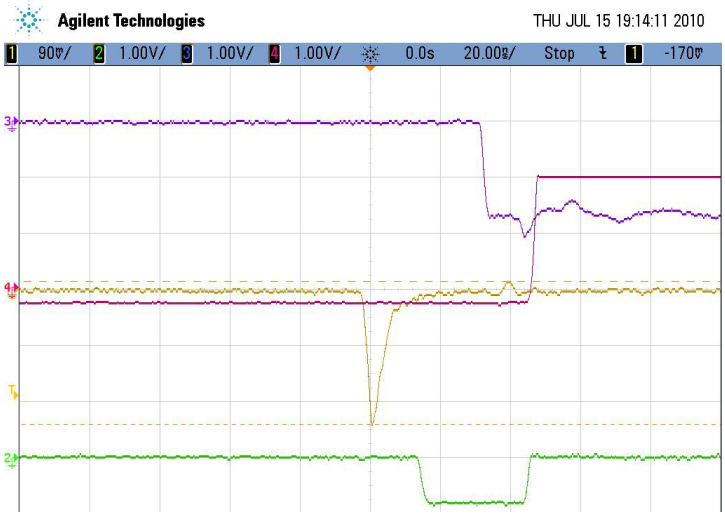

Figure 5.3: Comparison of signals: yellow - scintillator, green - discriminator, purple - dual timer, red - level adapter

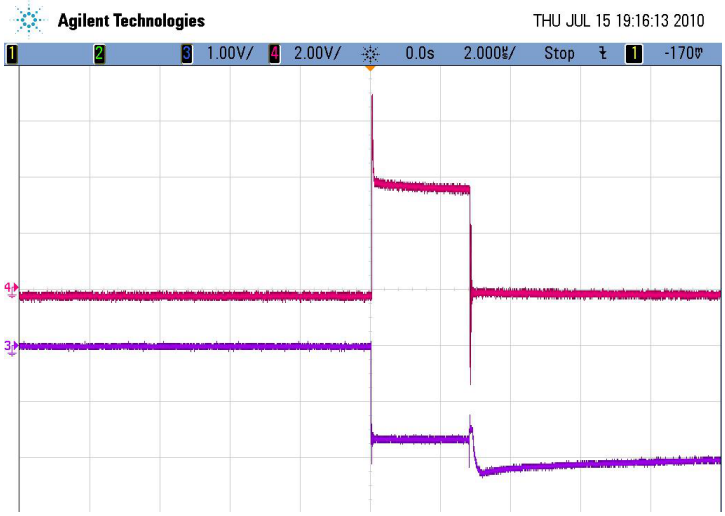

Figure 5.4: Comparison of signals: purple - dual timer, red - level adapter

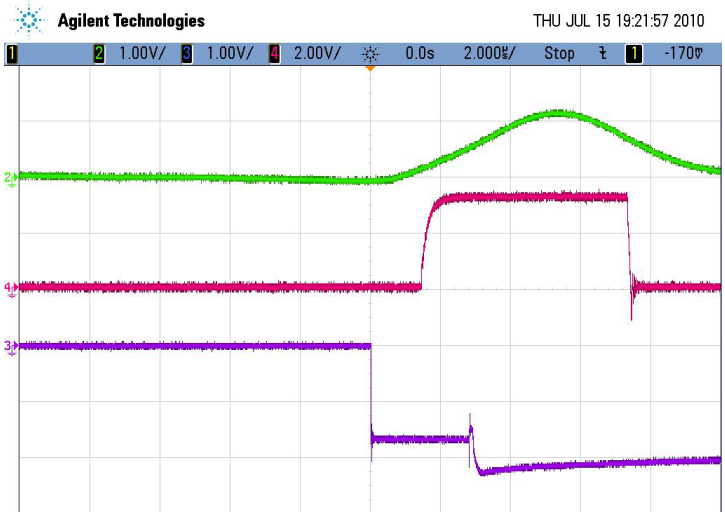

Figure 5.5: Comparison of signals: green - amplifier (diode detector), purple - dual timer, red - linear gate stretcher

scintillator trigger to gate in the signal from detector in ADC, which will be then process by multichannel readout PC. In the time sequence, the trigger signal must be present just before the peak maximum from the detectors signal as the height is equal to the energy of detected particle. To achieve

this, all particular signals were observed by oscilloscope and modified as desired by appropriate modules. For final shapes, timing and comparison of almost all signals see figures 5.2,5.3,5.4 and 5.5.

5.3 Measurements with radioactive source

First step is to choice the best silicon diode detector for the further testing. Thanks to a relatively large supply, 10 diodes without any surface damage or defects were picked and tested for their V/A characteristic (connected through preamplifier). Requirement is preferably linear characteristic to as high voltage as possible. The linear part of characteristic means fully depleted detector. Another plus is that the voltage fluctuation will cause no change in charge collection therefore from the examination of the diode V/A characteristic was determined the fixed value -70V for the power supply of the detector. Some other parameters were preset to a fixed value for all measurements or were tested in search for the best possible resolution and cooperation of modules. These values are summarized in the table 5.1 and V/A characteristic of the chosen diode is on figure 5.6.

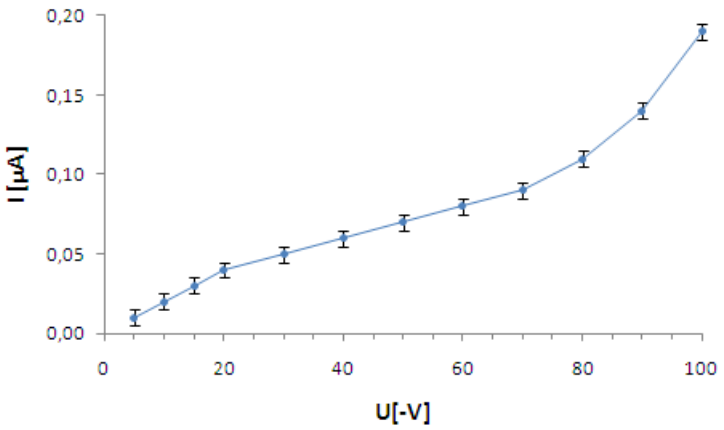

Figure 5.6: V/A characteristic of silicon diode - leakage current vs. bias voltage

MCA provides only sorting of incoming digital signals according to their height and total count for every pulse height is stored according for each am-

Shaping time (amplifier)	2μs
Gain (amplifier)	200
ADC gain	1000
MCA conversion gain	1024
threshold (discriminator)	-50mV

Table 5.1: Fixed values of fixed parameters

Half-life	Energies [MeV]	Branching
433 y.	5.486	85%
	5.443	13%

Table 5.2: Characteristics of ^{241}Am

plitude segment of the spectrum. Number of available channel into which the signals are separated is corresponding with MCA´s setting of *conversion gain*. This parameter influence the energy resolution of MCA module. Using calibration of well-known spectrum like ^{241}Am (α radioactive source) allows measuring of unknown spectrum. α decay is a two particle decay and due to this fact the alpha particles have a monoenergetic energy spectrum, which allows calibration of MCA´s channels for the energy measurement of continuous β^- spectrum. Advantage of this source is the energy value of α particles, which are safely above any possible noise. Properties of ^{241}Am are listed in the table 5.2 as is stated in [5]. The activity at the time of measurement was 1.26kBq.

Analyze of recorded spectrum of ^{241}Am shows peaks, which correspond with known values. Association of these provides channel calibration in first order. Every channel is now equal to interval of 0.00574 MeV. For measured alpha spectrum see figure 5.7.

Because of high noise level in low-energy part of spectrum, the grounding were paid special attention. This is due to the signal from the most energetic electrons, which deposit only minimum of energy by passing through the detector as was mentioned before. The grounding of preamplifier and the detector itself was remade several times to suppress the noise level as much as possible. Wiring with different diameter,length and made of various material was tested to ground one electrode of detector with the black box and installation. Preamplifier was finally wrapped in several layers of tinfoil. The noise level after grounding can be seen on figure 5.9 with overall improvement of at least three times against the original value. Grounding

successfully suppress count rate and maximum energy of the noise and thus allowing better detection for low energy particles.

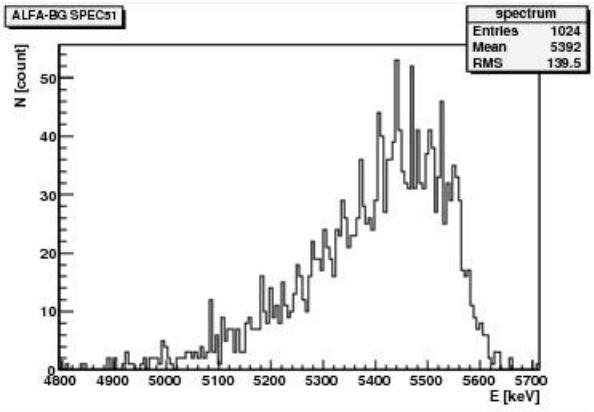

Figure 5.7: Energy spectrum with energy peaks of ^{241}Am (30 seconds measurement)

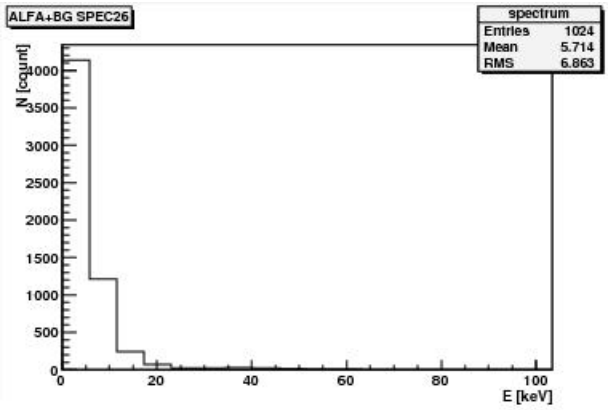

Figure 5.8: Noise after the upgrade of grounding (30 seconds measurement)

Firstly the background was obtained. One test is made with the same collimator as was used during measurement with the scintillator. In this case the effective distance between RS and detector is about 35mm (The collimator itself is adding 24mm). The second test is held without collimator so the distance is only 11mm. For both way is recorded one triggered spectrum (trigger value is fixed on the value -50mV) and one untriggered. Spectrum with collimator shows not only change of events intensity but also

changed shape of the spectrum and the mean energy as well. This indicates proper idea and right trigger timing. As was discussed in the beginning of this section, the untriggered spectrum is dominated by low energy electrons, while the triggered spectrum should be close to the Landau distribution of MIPs. In case of wrong timing, the triggered signal would belong to the previous/following particle and as the result the intensity of detected events will drop but the shape of the spectrum should remain the same.

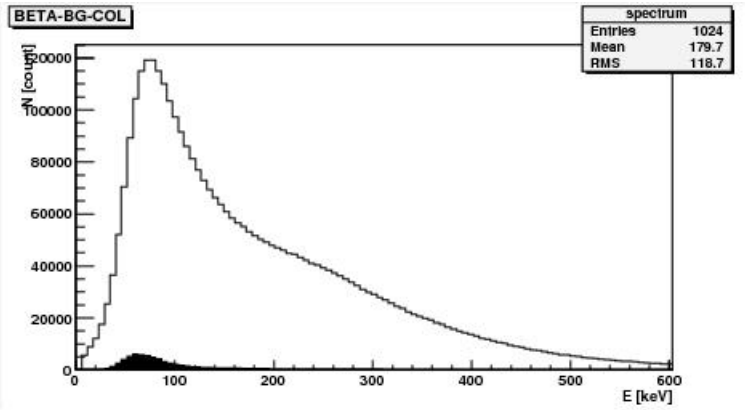

Figure 5.9: Deposited energy in silicon detector without collimator: outer histogram untriggered, inner triggered. (600 seconds measurements)

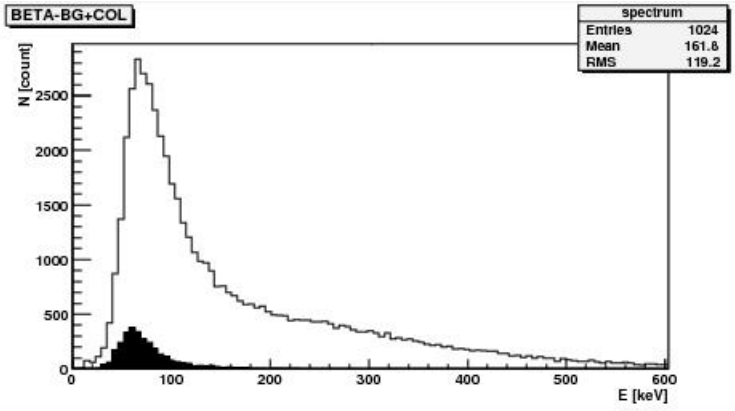

Figure 5.10: Deposited energy in silicon detector with collimator: outer histogram untriggered, inner triggered. (600 seconds measurements)

For measurements with collimator the mean deposited energy are (77,76±0,43)keV

for triggered and (169,20±0,86)keV for untriggered spectrum and for the measurements without collimator the mean deposited energy are (109,50±0,68)keV for triggered and (187,10±0,97)keV for untriggered spectrum.

Chapter 6

Measurement with microstrip detector via ALIBAVA system

The highly doped regions of detector (electrodes) may be segmented into strips (or pixels). When an ionizing particle passes through the detector, free electron-hole pairs are created and drift under the influence of the electric field in the depletion region. As a result a signal is induced on the electrodes in the near the spot of the original ionization. And finally the signal collected on the segmented electrodes provides information for the reconstruction of the original position of the particle. This is due to the fact, that the signal can be picked up on several electrodes and depending on the relative strength of the signals the interaction position of the particle can be determined. The silicon detector in this experiment has proportions of 1cm x 1cm with 300 μm thickness with 100 strips at a pitch of 80μm and it is p-type. The detector is mounted on the daughter board (supplies bias voltage for detectors) and connects to a Beetle amplifier chips.

The future aim of this experiment is to observe the signal spectra due to a minimum ionizing particle in a silicon detector and demonstrate the Landau distribution shape of collected charge if everything works fine. Second goal is to observe the physical size of a charge cluster from a minimum ionizing particle according to different geometries used in the experiment. This and future testing will allow testing of irradiated strip detectors for future upgrading of the LHC experiments or for development of new ones.

6.1 ALIBAVA description

ALIBAVA provides a compact and portable system for two different laboratory setups: 1) Laser system - synchronized trigger output generated internally for pulsing an external excitation source. 2) Radioactive source - external trigger input from one or two photomultipliers. The system is build around two front-end readout chips (Beetle chip used in LHCb) to acquire the detector signals. The ALIBAVA system is connected with PC via USB and allows online monitoring, calibration and changing parameters for measurement. The scheme for ALIBAVA connection can be seen on figure 6.1 [7].

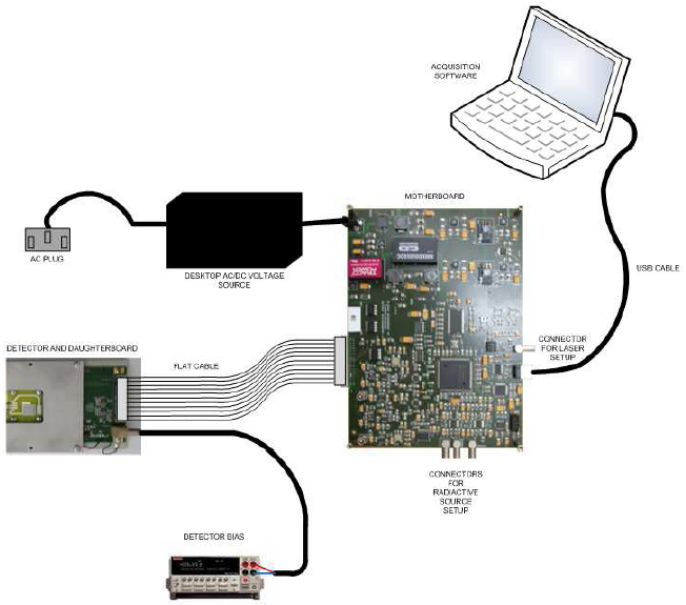

Figure 6.1: Picture of the module used in the experiment

The readout system of ALIBAVA consists of two different boards connected by flat cable. Daughter board and detector boards are fixed to base plate for facilitating wire-bonding. The reason for parting the hardware into two parts is to prevent the mother board from the hostile environment in which the detectors part will works. (High Radiation and possibly very low temperatures for better results). Daughter board supports two Beetle chips and has an additional amplifier to amplify the signal for transmission to the

mother board. It also contains fan-ins and detector support to operate the sensors. The Beetle chip is an analogue readout chip with 128 independent input channels and shaper with a 25ns peaking time. The used detector is a 1cm long ATLAS prototype silicon strip detector with 100 strips. The mother board accepts an analogue signal from trigger, digitizes the data and transfers it via the USB to the PC for further processing. The daughter board is shown on figure 6.2.

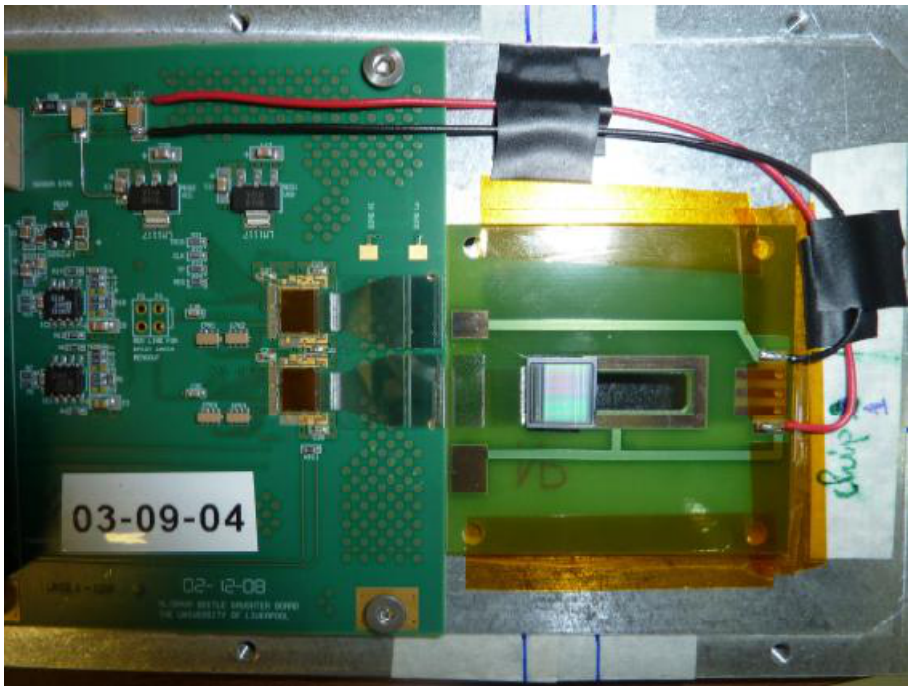

Figure 6.2: Daughter board

The detectors on the daughter board must be biased by an independent power supply. For this purpose the daughter board has a dedicated Lemo bias connector.

For measurement with a radioactive source the motherboard has three trigger inputs. The *TRIG IN1* and *TRIG IN2* trigger inputs are intended for signals coming from a photomultiplier. These inputs are discriminated using a onboarded discrimination level and can be used in coincidence (OR/AND). The *TRIG PULSE IN* input is intended for a digital current/voltage signal photomultiplier signal discriminated externally. The trigger signal is taken

from the same scintillator (with photomultiplier) as was used during previous experiments. For present experiment only one trigger signal is used. The schematic diagram for experiment is on figure 6.3. The ALIBAVA system has originally a silicon detector as a trigger but problems with motherboard firmware cause need to replace it with the fully compatible scintillator.

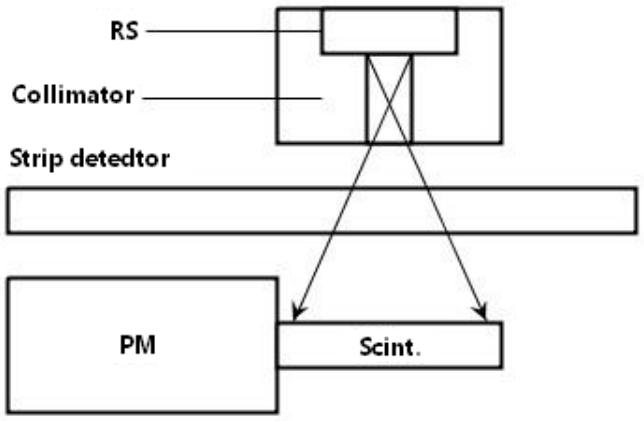

Figure 6.3: The schematic diagram for experiment

To find the signal in a given event, the signal collected on each given amplifier channel is compared in turn to a certain value called *seed cut*. If the value is higher than the cut, then the channel is considered to have signal. In that case the neighbouring channel is investigated. A new cut (inclusive cut) is applied to the neighbouring channel. If the second channel also overcomes this cut, the signal is then included into the whole event signal. This process is repeated until the signal on the neighbouring strip is below the inclusion cut. The signal size is the sum of the signals on all the strips in the cluster (strips with the signal) and the number of included strips is known as the cluster size. The applied cut must reduce the probability of including the noise, but at the same time should discard only minority of events.

6.2 ALIBAVA software

ALIBAVA system has two software parts. The data acquisition code to collect the data and perform online data analysis and the second data analysis

code to perform detailed off-line data analysis. Functions of the first part included controlling of the whole system (configuration, calibration and acquisition). Processing and monitoring of acquired data with the system interface (ALIBAVA-GUI). And finally generate the output files with binary data. For data analysis ALIBAVA provides a collection of root macros (still evolving) to read the data files and produce various histograms. Processing of data was carried out by Daniel Červenkov, who also programmed improved version of macros for data analysis. The ALIBAVA firmware provides generally 5 run modes but only two are important for the experiment: Pedestals for a pedestal run, source run in which the acquisition is triggered by signal above the threshold.

DAQ (data acquisition) configuration has a number of parameters inside the GUI:

- Sample size - this is the number of events stored in the mother board memory before sending them to the PC. This is only used in Pedestal, Laser and Source modes and is set to 100
- Number of events - desired number of detected and recorded events. All experiment runs are for 100,000 events
- threshold - value for successful triggering. The range was determined with regard to the scintillator testing as lies in range between -50mV and -250mV

The firmware provides variable graphs for online monitoring of measurement and checking if the output is not completly wrong. The graphs produced by ALIBAVA-GUI are:

- Signal – used for the calibration and radioactive source runs and is Only of interest for the radioactive source run.
- Pedestals and noise – used for the pedestal and radioactive source runs. This varies from channel to channel and event to event. The zero value is known as the pedestal. The noise on each channel is calculated by calculating the standard deviation of the signal (pedestal value) on that channel.
- Hitmap – shows the signal from the hit channels.
- Temperature – for eventual control of the daughterboard.

- Event display – this does not give the average but it displays the data on each channel for one last detected event
- Noise – the noise graph gives the average noise for each chip as a function of event number

Measurements of pedestals and noise graphs show difference between the two chips on the daughterboard as only one is connected to the detector so a larger noise signal is expected on one of them. A spikes above average indicates a noisy channel, while a very low spike indicates an unbonded channel. These channels should be masked out later to remove them from further testing. Also 28 channels need masking as only 100 strips is connected with the chip.

6.3 Measurements

For measurement was used the same β radioactive source (^{90}Sr) as for the previous measurements. The daughterboard is firmly connected with the detector plane and due to the delicate bounding covered in a compact box for protection. Special adjustable frame with a socket for different collimators is mounted above visible strip plane and scintillator. Frame allows to set the position of the RS towards the strips and scintillator. This can be particularly important for collimators with very small diameter as beam will hit only part of visible strips and consequently there should be a visible difference in signal.

For experiment were prepared two sets of collimators with three different size of diameter 1mm, 2mm and 5mm. One set is produced to have a perpendicular particle beam to the strips plane, while the second set is with 15° degree against the plane. The second set provide possibility to aim the beam either to has a perpendicular projection toward the strips or a collinear projection with the strips layout. The difference between the two sets should provide change of the energy spectrum as well as the cluster size. The reason is diverse tracks of the electrons in the detector.

The value range for the trigger is from the threshold -50mV to -250mV. These values are in correspondence with previous testing of the scintillator as the distance between the scintillator and the β source is 25mm. As the diameter of the collimators are 5mm, 2mm and 1mm, consideration about the rate of detected events must be made. Observation of testing with different power supply of the detectors for the same threshold level was planned.

K3	5mm diameter	perpendicular to the strips
K2	2mm diameter	perpendicular to the strips
K1	1mm diameter	perpendicular to the strips
U3-1	5mm diameter	15°, collinear projection
U2-1	2mm diameter	15°, collinear projection
U1-1	1mm diameter	15°, collinear projection
U3-2	5mm diameter	15°, perpendicular projection
U2-2	2mm diameter	15°, perpendicular projection
U1-2	1mm diameter	15°, perpendicular projection

Table 6.1: Properties of the collimators

So far more then 80 runs with different setting were made. See the table 6.1 for particular parameters of the collimators and the table 6.2 for listing of performed tests. Multiple pedestal runs for data analysis were also obtained. However the effect of various collimators is questionable as the side strips of the detector plane are covered by thin plastic foil due to the daughter-board mounting. Second unpleasant effect is the height of the collimators. With current geometry and proportions of collimators is no difference between 2mm and 5mm diameter as both particle beams are hitting all visible strips. Comparison of 1mm and 2mm will need future testing because of small comparable pool of tests.

The data were processed with improved macros for data analysis. Adaptation of macros and some proposal were made by Daniel Červenkov as was his bachelor thesis based on data analysis and angle dependence of cluster size etc. More information can be found in his bachelor thesis [2]. Part of the final root canvases are shown below on figure 6.4,6.5 and 6.6. For example cluster density, signal spectrum and others.

First available comparison is based on influence between value of the threshold level and median deposited energy in the detector for all three possible geometry (collimators with 5mm diameter). The trend is decreasing with higher threshold level as only more and more energetic particles activate the trigger according to the *section 3.6*, these electrons deposit the minimum of energy in the detector. The measurement for K3 collimator has the highest median energy as more particles with lower energy passes through detector and are triggered. But these deposit more energy in detector thus increasing the mean energy. For dependence see figure 6.7. The second figure 6.8 is showing the cluster size for the K3 and U3 collimators and in dependence

K3	K2	K1
threshold/detector voltage		
-50mV/-100V -80mV/-100,-50,-10,-5V -100mV/-100V -150mV/-100V -200mV/-100V -250mV/-100V	-50mV/-100V -80mV/-100,-50,-10,-5V -100mV/-100V -150mV/-100V -200mV/-100V -250mV/-100V	-50mV/-100V -80mV/-100,-50,-10,-5V -100mV/-100V -150mV/-100V -200mV/-100V -250mV/-100V
U3-1	U2-1	U1-1
threshold/detector voltage		
-50mV/-100V -80mV/-100,-50,-10,-5V -100mV/-100V -150mV/-100V -200mV/-100V -250mV/-100V	-50mV/-100V -80mV/-100,-50,-10,-5V -100mV/-100V -150mV/-100V -200mV/-100V -250mV/-100V	-50mV/-100V -80mV/-100,-50,-10,-5V -100mV/-100V -150mV/-100V -200mV/-100V -250mV/-100V
U3-2	U2-2	U1-2
threshold/detector voltage		
-50mV/-100V -80mV/-100,-50,-10,-5V -100mV/-100V -150mV/-100V -200mV/-100V -250mV/-100V	-50mV/-100V -80mV/-100,-50,-10,-5V -100mV/-100V -150mV/-100V -200mV/-100V -250mV/-100V	-50mV/-100V -80mV/-100,-50,-10,-5V -100mV/-100V -150mV/-100V -200mV/-100V -250mV/-100V

Table 6.2: Measurements with ALIBAVA taken so far

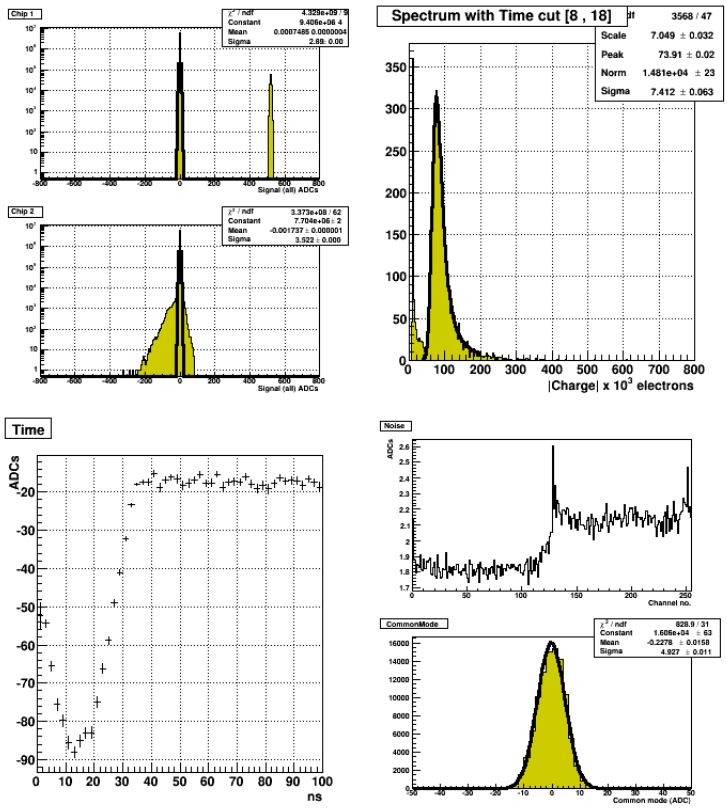

Figure 6.4: Final canvases from the macros like signal, noise, time profile of the signals etc.

with different values threshold levels. The cluster size is also dropping with higher threshold and the higher value is for U3-2 configuration, when the beam is aimed to hit more strips just by the geometry. The last two graphs represent dependence of mean energy and cluster size on voltage applied to the ALIBAVA detector as the voltage influence the depletion area and thus the charge collection efficiency. There is no surprise as both are dropping with lower voltage. The dependence is shown on figures 6.9 and 6.10.

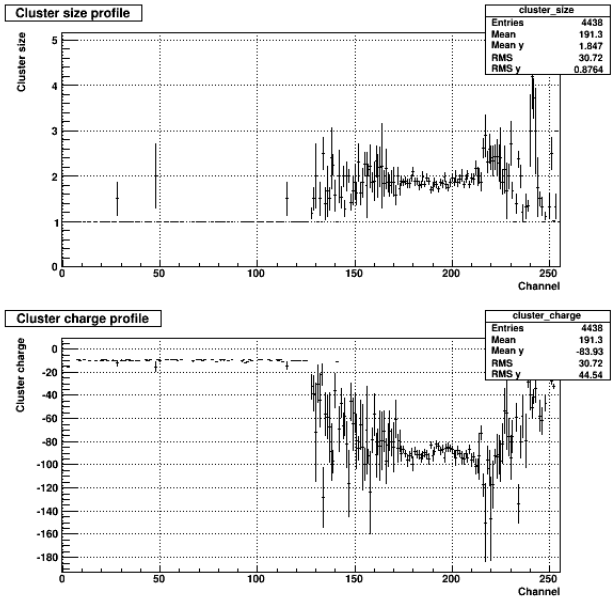

Figure 6.5: Cluster size profile top and cluster charge profile down.

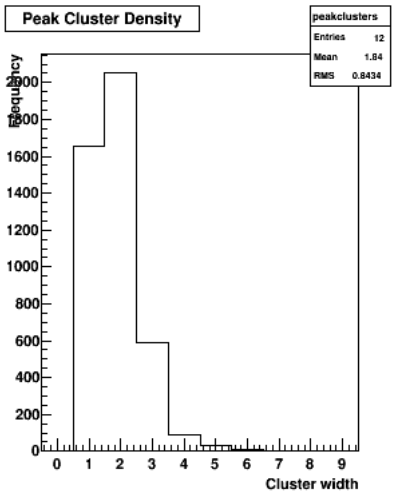

Figure 6.6: Peak cluster density.

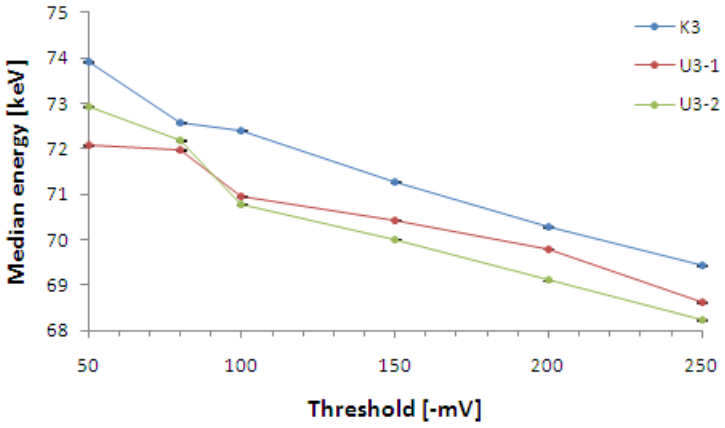

Figure 6.7: Mean deposited energy as function of threshold.

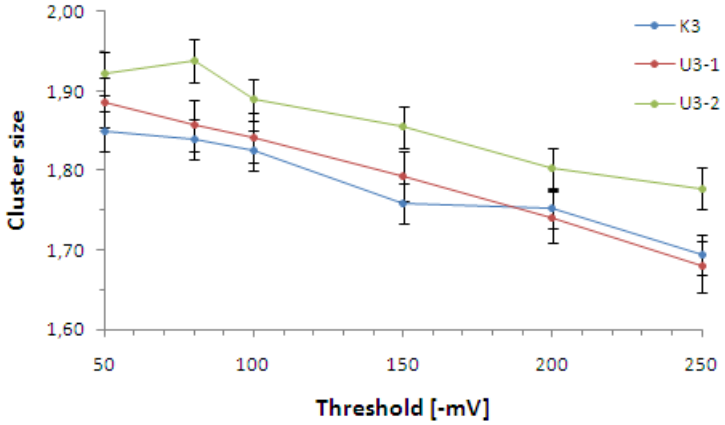

Figure 6.8: Cluster size as function of threshold.

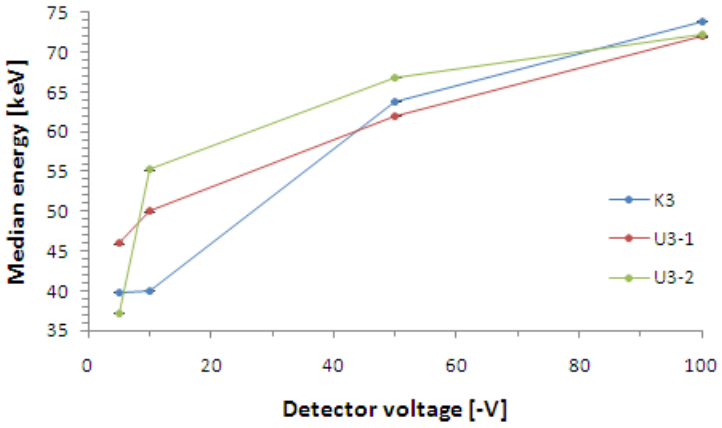

Figure 6.9: Mean deposited energy as function of detectors voltage.

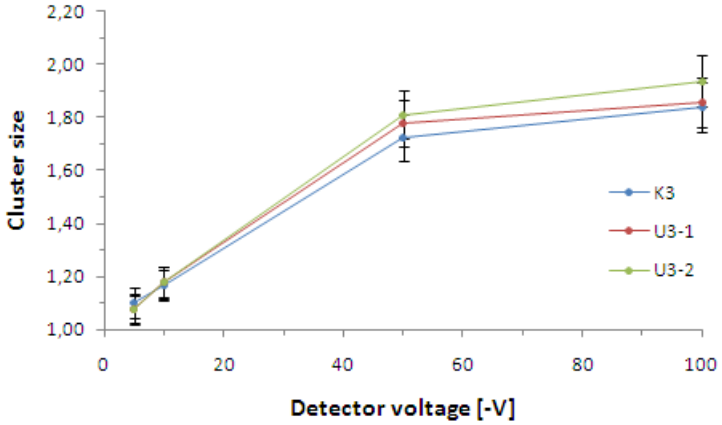

Figure 6.10: Cluster size as function of detectors voltage.

Chapter 7

Conclusion

The experiment with the scintillator was carried out and following analysis of results provided parameters for layout and geometry of next measurements with silicon detector and for measurements with ALIBAVA system where the same photosensor module with scintillator was used as part of the trigger. Black box also seems to provide enough shielding for our experiments from surrounding.

Experiment with silicon diode meets the expectations. Untriggered spectrum had broad deposited energy distribution, while with trigger is more likely Landau distribution of MIPs. Therefore testing with active trigger is more suitable for developing and testing new detectors as it simulates heavier charged particles.

The ALIBAVA system and first trial data were taken as was main aim of this part of the thesis. Data acquisition and data processing by root macros provided result in correspondence with expectations. With many observations and recommendations for future, the system is almost ready for detector testing. Changes will include the box for testing at the low temperatures and more complex mechanical part for angular testing etc.

Problem at the moment is an instability of the system. Usually after longtime measurements the change of setting (threshold,number events, etc.) results in GUI or motherboard giving an error. Official advise is to unplug the ALIBAVA and after plugging to restart the ALIBAVA and as the last part to launch the GUI.

Appendix A

Photodocumentation

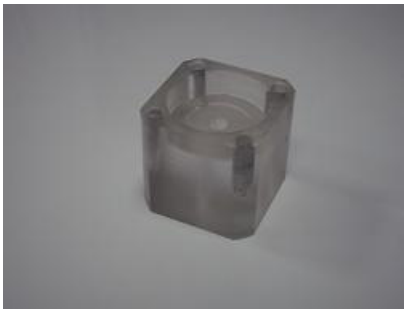

Figure A.1: Collimator for scintillators and diode testing with RS.

Figure A.2: Set of 6 collimators for the ALIBAVA testing.

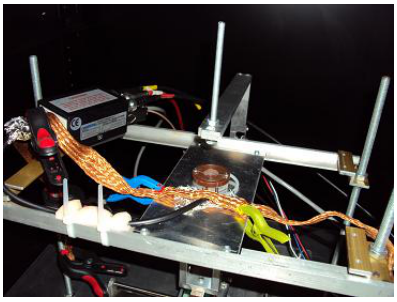

Figure A.3: Diode with grounding, collimators fixation and preamplifier.

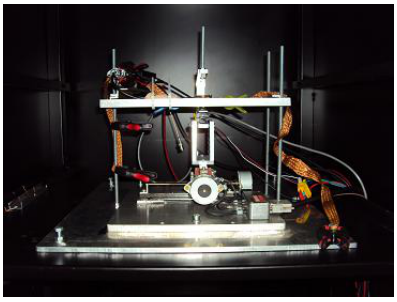

Figure A.4: Whole apparatus for diode testing.

Figure A.5: The look at the whole laboratory with a black box.

Figure A.6: All modules for experiments and power supply for the PM.

Figure A.7: The multichannel readout analyzer and oscilloscope.

Figure A.8: Modules and ALIBAVA motherboard in the box.

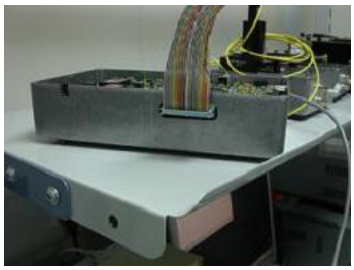

Figure A.9: Opened ALIBAVA motherboard box.

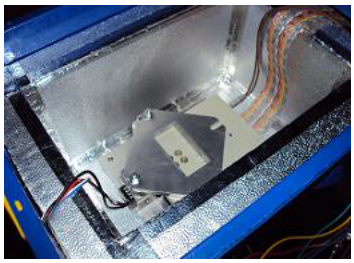

Figure A.10: Box with daughterboard and detectors plane.

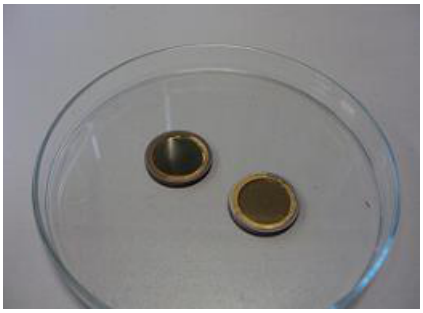

Figure A.11: Silicon diodes as the one used for the experiment.

Bibliography

[1] Broklová Z.: *Efficiency and quality evaluation of ATLAS semiconductor strip detectors for LHC at CERN*, thesis at Faculty of Mathematics and Physics at Charles University, Prague, 2003

[2] Červenkov D.: *Tests of silicon detectors for particle physics experiments*, thesis at Faculty of Mathematics and Physics at Charles University, Prague, 2010

[3] Doležal Z.: *Systematic effects in some semiconductor detector tests*, Nuclear Instruments and Methods, A583 37-41, 2007

[4] Hamamatsu Corporation: *http://pdf1.alldatasheet.com/datasheet-pdf/view/62580/HAMAMATSU/H5783-01.html*

[5] Amsler C.: *et al.*, *Particle Physics Booklet*, CERN, Geneva, 2008

[6] J. Garcia: *XI ICFA School on Instrumentation in Elementary Particle Physics*, San Carlos de Bariloche, 2010

[7] Marco-Hernanández R.: *Performance of the ALIBAVA system with irradiated and non-irradiated microstrip silicon sensors*, PoS(EPS-HEP), 152, 2009

[8] Kittel C.: *Introduction to Solid State Physics*, John Wiley and Sons, New York, 1996

[9] Knoll G. F.: *Radiation detection and measurement*, John Wiley and sons, 1979

[10] Leo W.R.: *Techniques for Nuclear and Particle Physics Expriments*, Springer-Verlag, 1994

[11] Lutz G.: *Semiconductor Radiation Detectors*, Springer, Berlin, 1999

[12] Řezníček P.: *Tests of semiconductor microstrip detectors of ATLAS detector*, thesis at Faculty of Mathematics and Physics at Charles University, Prague, 2003

[13] Sauli F.: *Instrumentation In High Energy Physics*, World Scientific Publishing Co. Pte .Ltd., Singapore,1993